

PACS numbers: 77.22. – d, 77.22.Ch, 77.22.Gm

**STRUCTURAL, OPTICAL, AND DIELECTRIC PROPERTIES OF
A(Mg_{0.32}Co_{0.02})Nb_{0.66}O₃ SEMICONDUCTOR, WHERE (A = Ba, Sr or Ca)**

B. Bishnoi¹, P.K. Mehta¹, C.J. Panchal², M.S. Desai², R. Kumar³

¹ Department of physics, Faculty of Science,
The M.S. University of Baroda, Vadodara-390002, Gujarat, India
Email: pkmehta_phy@yahoo.co.in

² Applied Physics Department, Faculty of Technology & Engineering,
The M.S. University of Baroda, Vadodara-390001, Gujarat, India
Email: cjpanchal_msu@yahoo.com

³ Head, Material Science Division, National Institute of Technology,
Hamirpur-177005, Himachal Pradesh, India

Structural optical and dielectric properties of single phase A(Mg_{0.32}Co_{0.02})Nb_{0.66}O₃, where A = Ba, Sr, or Ca, compounds were studied in the temperature range from room temperature (293 K) to 458 K. The X-ray diffraction revealed that the Ba(Mg_{0.32}Co_{0.02})Nb_{0.66}O₃ [BMCN] compounds exhibit hexagonal symmetry whereas Sr(Mg_{0.32}Co_{0.02})Nb_{0.66}O₃ [SMCN] and Ca(Mg_{0.32}Co_{0.02})Nb_{0.66}O₃ [CMCN] compounds exhibit monoclinic symmetry. The replacement of Barium ($r = 1.61 \text{ \AA}$) by smaller ions like Strontium ($r = 1.44 \text{ \AA}$) or Calcium ($r = 1.34 \text{ \AA}$) in the polar dielectric Ba(Mg_{0.32}Co_{0.02})Nb_{0.66}O₃ introduces the relaxation phenomenon and a gradual increase in the transition temperature maximum (T_m). The ac conductivity, as determined from the dielectric data, as a function of temperature and frequency, reveals the crossover from small polaron tunneling (SPT) to correlated barrier hopping (CBH) type conduction at $\approx 370 \text{ K}$. The activation energy of the non-Debye type process evaluated both from the electric modulus and the conductivity data are nearly identical suggesting similarity in the hopping mechanism. The band gap of these materials lies in the range of narrow to wide band semi conductors.

Keywords: X-RAY DIFFRACTION, BAND GAP, DIELECTRIC PROPERTIES, AC CONDUCTIVITY, 1:2 NIOBATES.

(Received 04 February 2011, in final form 14 October 2011)

1. INTRODUCTION

Perovskite oxides are of great interest due to their varied physico-chemical properties and wide applications. The crystal structure and physical properties such as ferroelectricity, antiferroelectricity, and piezoelectricity, are influenced by the ionic displacement. The effect of structural changes accompanied by the octahedral tilting have attracted much attention owing to their effects on the behavior of temperature-dependent conductivity in low dielectric loss materials [1-3].

Recently, structural investigations on Ba(Mg_{1/3}Nb_{2/3})O₃, [BMN], Sr(Mg_{1/3}Nb_{2/3})O₃, [SMN], and Ca(Mg_{1/3}Nb_{2/3})O₃, [CMN] have been reported [4-6]. An anti-phase, in-phase tilting of oxygen octahedral was reported in SMN and CMN systems [7]. Attempts were made to study the ac conductivity and the dielectric relaxation in SMN and CMN compounds [8, 9]. No

significant efforts are carried out to correlate the A-site substitution induced structural disorder with dielectric relaxation. In the present work, we show the correlation between substitution-induced structural transition and polar to non-polar type dielectric transition in these modified systems. Further, it is necessary to analyze the dielectric relaxation and the ac conductivity as a function of temperature in order to identify the exact mechanism of conduction and the nature of dipolar coupling. Our studies on Sr[(Mg_{0.32}Co_{0.02})Nb_{0.66}]O₃, SMCN thin films exhibited a significant sudden jump in the activation energy at ~ 370 K [10]. Its origin needed further analysis.

In this paper, we have investigated the structural and electrical properties of A[(Mg_{0.32}Co_{0.02})Nb_{0.66}]O₃; A = Ba, Sr or Ca, by means of X-ray diffraction (XRD) and dielectric spectroscopy. In the above samples, optimum doping of ~ 1 % cobalt at B-site is observed to enhance the Q-factor and also lower the phase formation temperature of the sample to 1100-1200 °C. In the present study we have observed a wide variations in band gap as well as transition in dielectric properties from normal to colossal values (~ 10²) as well as occurrence of dielectric relaxation due to A-site modification in Ba[(Mg_{0.32}Co_{0.02})Nb_{0.66}]O₃. A number of parameters associated with the dielectric relaxation behavior as well as frequency response to the conductivity have been determined and discussed herein. The above-mentioned sudden change in the activation energy ~ 370 K [10] is to be correlated with the change in ac conductivity mechanism.

2. EXPERIMENTAL

The Ba[(Mg_{0.32}Co_{0.02})Nb_{0.66}]O₃, [BMCN], Sr[(Mg_{0.32}Co_{0.02})Nb_{0.66}]O₃, [SMCN], and Ca[(Mg_{0.32}Co_{0.02})Nb_{0.66}]O₃, [CMCN] compounds were prepared by using a two-stage synthesis process. In the first stage, [(Mg_{0.32}Co_{0.02})Nb_{0.66}]O₃ precursor phase was produced from MgO (≥ 99%), CO₃O₄(≥ 99%), Nb₂O₅ (≥ 99%) powders taken in stoichiometric proportions. The powders are mixed homogeneously, pressed lightly into pellets, and calcined at 900°C for 6 h. After the initial precursor heating cycles, in the second stage a stoichiometric amount of BaCO₃, SrCO₃, or CaCO₃ were thoroughly mixed and calcined at 900°C to decompose the carbonate.

Prior to each heating cycle, the samples were grinded and pelletized using an uniaxial press. Multiple heating cycles, with intermediate grindings and re-pelletization were performed in the temperature range of 900 °C to a final temperature of 1200°C. In each cycle, sintering is carried out in air for 12 hrs.

X-ray diffraction (XRD) measurements were carried out on powdered samples using a high resolution Shimadzu X-ray diffractometer 6000 using CuK_α radiation (λ = 1.5402 Å). The diffraction patterns were recorded from 2θ = 10 ° to 110 ° with a step of 0.02 °. The UV/VIS Spectra was measured by Perkin Elmer Precisely Lambda 950 instrument. Its range was from 300-1500 nm. All the measurement were carried out in Reflectance mode. The temperature-dependent dielectric measurements were carried out using an LCR meter (1260 Solartron) having frequency range of 10²-10⁷ Hz. The A[(Mg_{0.32}Co_{0.02})Nb_{0.66}]O₃ samples (thickness 1.18 mm and diameter of 12 mm) were polished with silver paste and heat-treated at 200 °C in order to remove micro-cracks (if any). Polished discs were placed between two electrodes connected to an LCR meter and measurements were performed from room temperature to 180 °C; the results were reproducible. The dc conductivity was calculated using the Cole-Cole plot.

3. RESULTS AND DISCUSSIONS

3.1 XRD analysis

XRD patterns of $A[(Mg_{0.32}Co_{0.02})Nb_{0.66}]O_3$ at room temperature are shown in Fig. 1. All the reflection peaks of the X-ray profile are indexed using the least-square method with the help of the standard indexing program "Powder-X". It is evident that the XRD peaks shifted toward higher 2θ angle on replacement of Sr^{2+} or Ca^{2+} at the A-site (Ba^{2+}). The calculated lattice parameters are listed in Table 1.

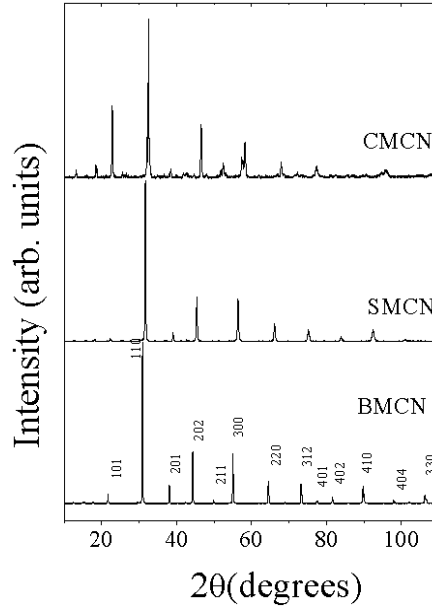


Fig. 1 – X ray diffraction patterns of BMCN, SMCN, and CMCN

Table 1 – The lattice Parameter, Unit cell Volume and relaxation activation energy for $A[(Mg_{0.32}Co_{0.02})Nb_{0.66}]O_3$

Composition	Structure	Lattice parameter	Volume of unit cell	Activation Energy
$Ba[(Mg_{0.32}Co_{0.02})Nb_{0.66}]O_3$ [BMCN]	hexagonal	$a = 5.766 \text{ \AA}$ $b = 5.766 \text{ \AA}$ $c = 7.077 \text{ \AA}$	236.45 \AA^3	-
$Sr[(Mg_{0.32}Co_{0.02})Nb_{0.66}]O_3$ [SMCN]	monoclinic	$a = 8.956 \text{ \AA}$ $b = 13.461 \text{ \AA}$ $c = 5.778 \text{ \AA}$ $\gamma = 93.33$	696.64 \AA^3	0.164 eV
$Ca[(Mg_{0.32}Co_{0.02})Nb_{0.66}]O_3$ [CMCN],	monoclinic	$a = 10.965 \text{ \AA}$ $b = 13.463 \text{ \AA}$ $c = 5.875 \text{ \AA}$ $\beta = 125$	867.65 \AA^3	0.185 eV

The X-ray diffraction analysis reveals that the hexagonal structure of BMCN modifies to a lower symmetric monoclinic structure in SMCN and CMCN samples. The increase in asymmetry was accompanied by the simultaneous increase in the cell volume [4]. In earlier work researchers have observed an anti-phase tilting of the oxygen octahedral in SMCN and an anti-phase/in-phase tilting of the oxygen octahedral accompanied by an anti-parallel shift of A-site cations in CMCN compounds [7]. The observed enhancement in distortions can have correlated variations in the dielectric properties of these compounds.

3.2 UV/VIS Spectroscopy

The direct and indirect band gap values of these compounds are shown in Table 2. It is clear from band gap values, which goes on increasing on reducing the ionic radii, that on replacing the Ba²⁺ by Sr²⁺ and Ca²⁺ the system moves from the narrow band gap to wide band gap semi conducting region. Thus, isovalent substitutions in above 1:2 type Niobates provides a useful way to produce a semiconducting device with desirable band gap.

Table 2 – Band gap of BMCN, SMCN and CMCN

Composition	Direct Band Gap	Indirect Band Gap
BMCN	1.14	1.13
SMCN	3.0	2.91
CMCN	3.39	3.2

3.3 Electrical Measurement

3.3.1 Dielectric permittivity measurements

Fig. 2 and 3 show the real and imaginary parts of the dielectric constant as a function of frequency in BMCN, SMCN, and CMCN samples. In order to

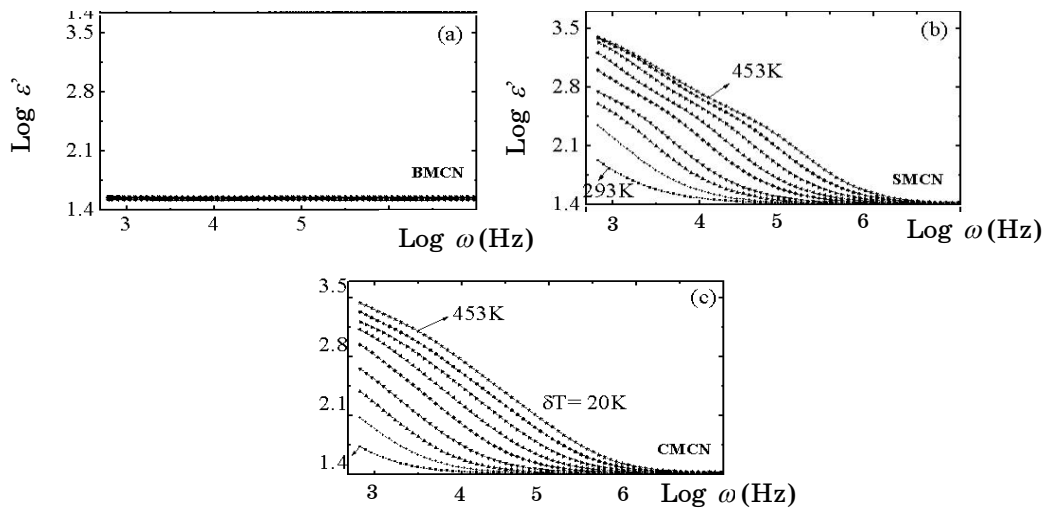


Fig. 2 (a-c) – Angular Frequency dependence of the real part (ϵ') of the electrical permittivity for different compositions

study the effect of A-site structural modifications on the dielectric properties of the substituted niobates we have used impedance spectroscopy. The complex dielectric permittivity $\varepsilon^*(\omega)$ is defined as,

$$\varepsilon^*(\omega) = \varepsilon'(\omega) + i\varepsilon''(\omega) \quad (1)$$

As BMCN is a polar dielectric material, the real dielectric constant remains independent of frequency $\{\varepsilon'(\omega) \sim 34\}$. On the other hand replacement of Ba^{2+} by Sr^{2+} or Ca^{2+} in $\text{A}[(\text{Mg}_{0.32}\text{Co}_{0.02})\text{Nb}_{0.66}]\text{O}_3$, the real dielectric constant shows a strong frequency dispersion at room temperature. This implies that the material exhibits a transition from polar to non-polar dielectrics.

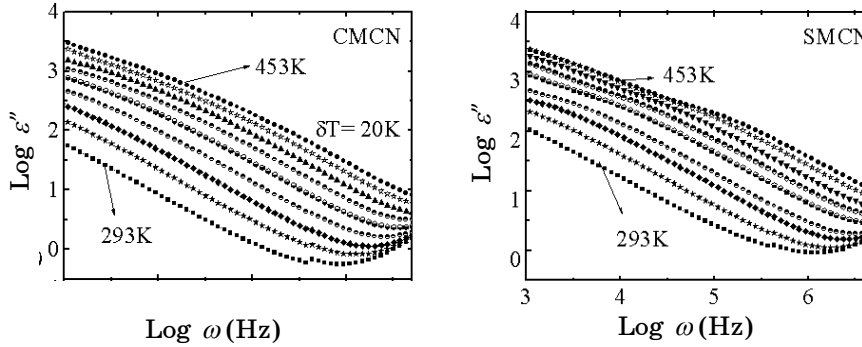


Fig. 3 – Angular Frequency dependence of the complex part (ε'') of the electrical Permittivity for different compositions

Fig. 4 shows the temperature-dependence of the dielectric constant ε' measured at various frequencies (100 Hz to 32 MHz). We have observed a transition in dielectric properties from normal to colossal values ($\sim 10^3$) as well as occurrence of dielectric relaxation due to A-site modification in $\text{Ba}[(\text{Mg}_{0.32}\text{Co}_{0.02})\text{Nb}_{0.66}]\text{O}_3$. The present results indicate strong correlation between the dielectric properties and the structural modifications around the A-site in $\text{A}[(\text{Mg}_{0.32}\text{Co}_{0.02})\text{Nb}_{0.66}]\text{O}_3$ compounds.

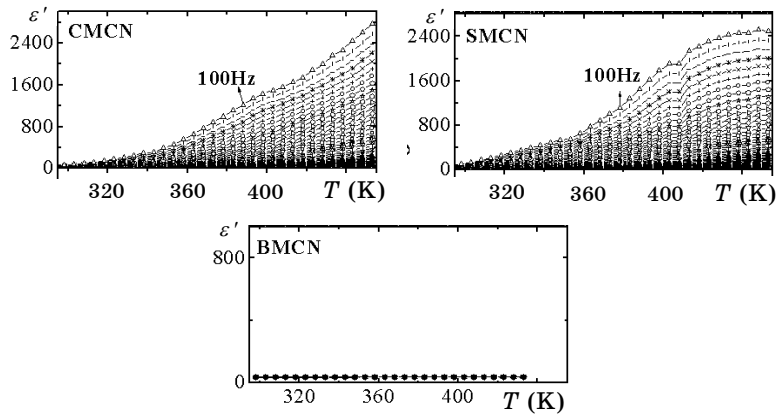


Fig. 4 – Temperature dependence of the real part (ε') of the electrical permittivity for different frequencies

3.3.2 Electric Modulus Measurement

In the absence of well-defined dielectric-loss-peak, the relaxation mechanism can be determined with the help of electric modulus $M^*(\omega)$, which is defined in terms of the complex dielectric permittivity ϵ^* by the relation,

$$M^* = 1/\epsilon^* = M'(\omega) + iM''(\omega) \quad (2)$$

Where $M'(\omega)$ and $M''(\omega)$ are the real and imaginary parts of $M^*(\omega)$ and are defined as,

$$M'(\omega) = \epsilon' / [(\epsilon')^2 + (\epsilon'')^2] \quad (3)$$

$$M''(\omega) = \epsilon'' / [(\epsilon')^2 + (\epsilon'')^2] \quad (4)$$

We have adopted the modulus formalism to study the relaxation mechanism only in SMCN and CMCN. In polar-type dielectrics (BMCN) the relaxation phenomenon is absent. Fig. 5 shows the real and imaginary components of the electric modulus as a function of frequency for CMCN in the temperatures range from room temperature to 453 K. It is evident from Fig. 5(a) that the real part of the electric modulus, $M'(\omega)$, exhibits a dispersion and approaches to M_∞ (the asymptotic value of $M'(\omega)$ at higher frequencies); whereas the imaginary part of electric modulus, $M''(\omega)$, Fig. 5(b), exhibits a maximum (M''_{\max}) centered at the dispersion region of $M'(\omega)$. The observed shift in M'' towards higher relaxation frequencies with rise in temperature implies that the spectral intensity of the dielectric relaxation is thermally activated.

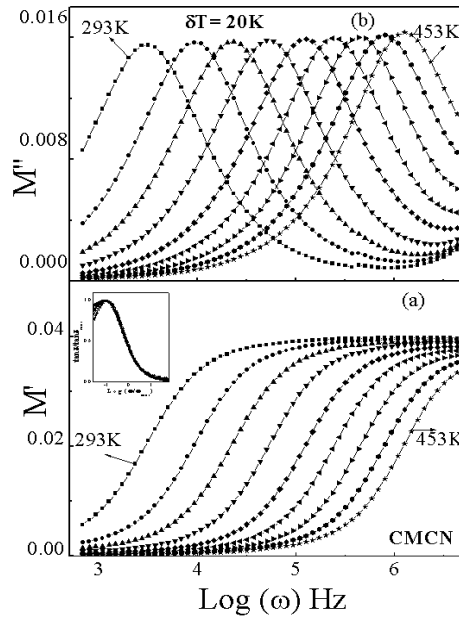


Fig. 5 – Angular Frequency dependence of the electrical Moduli (M') and (M'') at different temperatures CMCN

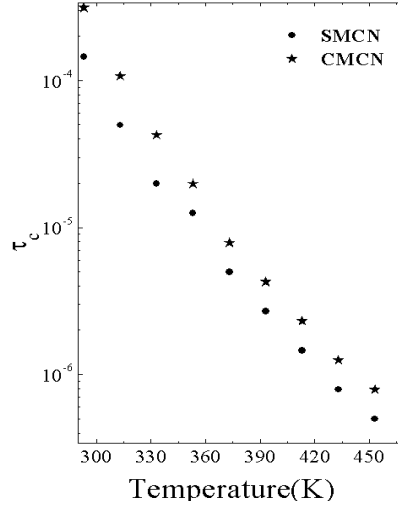


Fig. 6 – The temperature dependence of Relaxation time of SMCN and CMCN

Further, inset in Fig. 5(a) shows a peak in dielectric-loss whose dispersion indicates that varying mechanisms operating at different temperatures in CMCN. This type of behavior may be due to the hopping of charge carriers and the dominance of intrinsic small polarons [11]. It is known that the frequency region below M''_{\max} is identified with the long-range hopping of charge carriers while above M''_{\max} is linked to the short-range hopping of small polarons. Here the carriers were expected to be confined to potential wells, being mobile for only short distances. We have observed a similar behavior in SMCN compound. Fig. 6 shows the temperature-dependence of relaxation time for SMCN and CMCN. The relaxation time, τ_c , at a given temperature, is calculated by taking the frequency, ω_c , corresponding to M''_{\max} and using the relation $\omega_c \tau_c = 1$. In both these samples, relaxation time decreases with increase in temperature. The relaxation in CMCN is more than that of SMCN. It appears that the enhanced structural disorder in the form of anti-parallel shift and/or in-phase tilting of oxygen octahedral in CMCN causes further softening of the dipolar coupling.

We have also attempted to calculate the thermal activation energy using the electric modulus data using the following Arrhenius relation:

$$\omega = \omega_0 \cdot \exp[E_{relax}/(k_B T)] \quad (5)$$

The slope of the linear fit for the above relation directly provides the measure of the activation energy, E_{relax} . Fig. 7 shows the log-log plot of ω_{\max} vs $1/T$ (K^{-1}) for CMCN. The calculated activation energy for relaxation phenomenon are given in Table 1. To validate that the dynamical processes in these materials below ferroelectric transition temperature are independent of temperature, we have performed the scaling of imaginary part of electric modulus as a function of frequency at different temperatures. Fig. 8(a) and 8(b) show the $M''(T)/M''_{\max}(T)$ as a function of $\omega/\omega_{\max}(T)$ for CMCN and SMCN. From Fig. 8 it is evident that all the curves corresponding to different temperatures overlap into a single master curve indicating that the dynamical processes are temperature- independent [12].

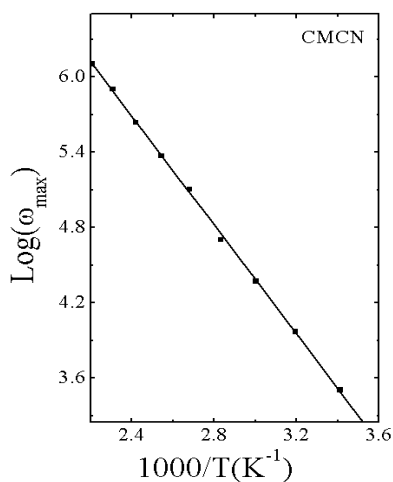


Fig. 7 – The Arrhenius plot of relaxation frequency (ω_{max}) for CMCN as a function of temperature. The crosses represent the experimental points and the least-squares fit is shown by solid line

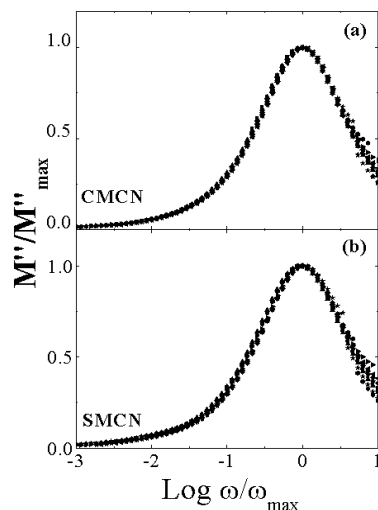


Fig. 8 – Plot of scaling behaviour of M'' for different compositions as a function of temperature

3.4 AC Conductivity measurements

The ac conductivity (σ_{ac}) was studied over a frequency range of 100 Hz to 32 MHz as well as varying the temperature from room temperature to 458 K. Fig. 9 shows that the σ_{ac} calculated from the dielectric data, using the following equation,

$$\sigma_{ac} = \varepsilon_0 \varepsilon' \omega \tan \delta \quad (6)$$

increases for A[(Mg_{0.32}Co_{0.02})Nb_{0.66}]O₃ samples and is distinct in the high frequency region.

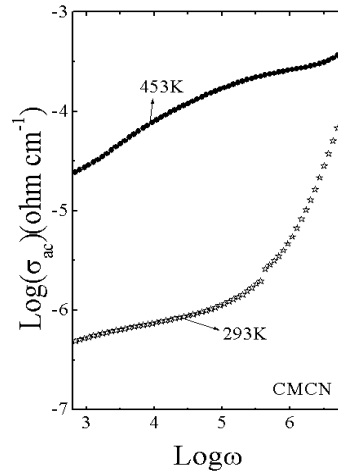


Fig. 9 – Frequency dependence of ac conductivity of CMCN at different temperatures. Straight lines are obtained by least-square fitting. The slopes of respective lines gave the values of the frequency exponent s

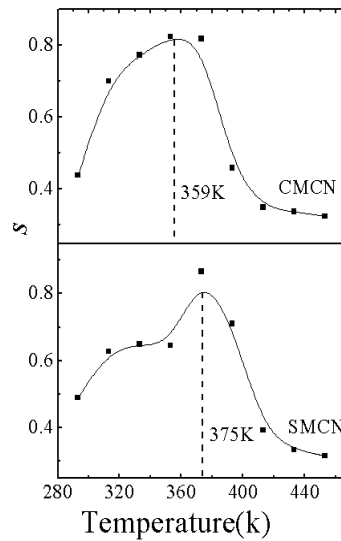


Fig. 10 – Temperature dependence of the frequency exponent s .

This indicates that the hopping frequency of the charge carriers is influenced by the neighbors of Sr^{2+} or Ca^{2+} ions. Further, it is noted that at higher frequencies (~ 2 MHz), σ_{ac} decreases for all compositions indicating the inability of hopping of charges to follow the high frequency of the applied field.

The total conductivity of the material at a given frequency is given by,

$$\sigma_{total}(\omega) = \sigma_{dc}(\omega) + \sigma_{ac}(\omega) \quad (7)$$

where, hopping-induced conduction arising from A-site substitutions is responsible for the enhancement of both dc and ac conductivities. The dc conductivity is the $\omega \rightarrow 0$ limit of $\sigma_{\text{total}}(\omega)$. For semiconductors and disordered systems, the ac conductivity follows the power law behavior:

$$\sigma_{ac}(\omega) = A \omega^s \quad (8)$$

Where A is a temperature-dependent constant and s is the frequency exponent ($s \leq 1$). From the slope of log-log plots drawn for σ_{ac} vs. ω (Fig. 9), for the different compositions at room temperature, the slope directly provides the value of dimensionless frequency exponent s . The ac conductivity shows frequency-dependent dispersion similar to the dielectric behavior discussed earlier. The temperature-dependence of frequency exponent s representing a measure of correlation between σ_{ac} and frequency is shown in Fig. 10. It exhibits a transition from gradually enhancing nature of s to decreasing type at around 370 K. Such a thermally activated behavior of s according to small polaron tunneling model (SPT) indicates that the conductivity is due to polarons, independent of the inter-site separation [13]. On the other hand, for temperatures beyond 370 K, the decreasing nature of s is inferred from the correlated barrier-hopping model (CBH) [14]; here, the conduction is due to electron transfer over the barrier between two sites having their own columbic potential wells. The CBH model is of particular interest as it explains the conductivity mechanism in systems investigated here, in which the dc conductivity is not negligible. We also note the significance of transition from SPT type conduction behavior to CBH type conduction at ~ 370 K in the form of observed ‘‘Switching behavior’’ in the thin films of SMCN at the same temperature [10].

4. CONCLUSIONS

Substitutions of smaller ions Sr²⁺ and Ca²⁺ at Ba²⁺- site in Ba[(Mg_{0.32}Co_{0.02})Nb_{0.66}]O₃ drives the structure towards lower symmetry (Hexagonal to monoclinic). It simultaneously changes Polar dielectric BMCN to a relaxor dielectric in SMCN and CMCN. Increase in structural asymmetry gradually enhances the unit cell leading to correlated enhancement in dielectric constant ϵ' . Dielectric loss $\tan\delta$ is nearly same for Sr and Ca substituted compounds, but $\tan\delta$ gradually increases (Ba \rightarrow Sr \rightarrow Ca). Both SMCN and CMCN exhibits enhancement in relaxation time with temperature suggesting systematic softening of dipolar coupling. SMCN as well as CMCN exhibits a significant transition in conductivity behavior from small polaron tunneling (SPT) type to Correlated Barrier Hopping (CBH) type ~ 370 K. This temperature coincides well with our earlier reported switching behavior in activation energy of SMCN thin films. Thus above niobate system possessing wide semi- conducting band gap region and conductivity mechanism based switching behavior is an ideal candidate for sensor, optoelectronic, and electrical switching device applications.

One of the authors (B.S. Bishnoi) is thankful to Inter University Accelerator Centre (IUAC) formerly known as Nuclear Science Centre (NSC) New Delhi, India for providing her financial support through Project No. UFUP-41315. Some of the authors¹ are thankful to UGC DRS Program for funding experimental facilities in the Department.

REFERENCES

1. E.L. Colla, I.M. Reaney, N. Setter *J. Appl. Phys.* **74**, 3414 (1993).
2. M.A. Akbas, P.K. Davies, *J. Am. Ceram. Soc.* **81**, 670 (1998).
3. A.J. Bosman, E.E. Havinga, *Phys. Rev.* **129**, 1593 (1963).
4. S.M. Gupta, E. Furman, E. Colla, Z. Xu, D. Viehland, *J. Appl. Phys.* **88**, 2836 (2000).
5. H.J. Lee, H.M. Park, Y.K. Cho, Y.W. Song, S. Nahm, J.D. Byun, *J. Am. Ceram. Soc.* **84**, 3032 (2001).
6. H.J. Lee, H.M. Park, Y.K. Cho, Y.W. Song, S. Nahm, J.D. Byun, *J. Am. Ceram. Soc.* **84**, 1632 (2001).
7. C.S. Park, J.H. Paik, S. Nahm, H.J. Lee, H.M. Park, K.Y. Kim *J. Mater. Sci. Lett.* **18**, 691 (1999).
8. A. Dutta, C. Bharti, T.P. Sinha, *Physica B* **403**, 3389 (2008).
9. A. Dutta, C. Bharti, T.P. Sinha *Mater. Res. Bull.* **43**, 1246 (2008).
10. P.K. Mehta, B. Bishnoi, R. Kumar, R.J. Choudhary, D.M. Phase, *Solid State Phenom.* **155**, 145 (2009).
11. K. Prabakar, S.A.K. Narayandass, D. Mangalaraj, *Cryst. Res. Technol.* **37**, 1094 (2002).
12. S. Saha, T.P. Sinha, *Phys. Rev. B.* **65**, 134103 (2002).
13. D. Emin, T. Holstein, *Ann. Phys.* **53**, 439 (1969).
14. G.E. Pike, *Phys. Rev. B.* **6**, 1572 (1972).
15. S.R. Elliot, *Philos. Mag.* **36**, 1291 (1977).